International Journal of Environmental Science and Technology (2021) 18:2125–2136
https://doi.org/10.1007/s13762-020-02968-7

ORIGINAL PAPER

Equilibrium, kinetic, and diffusion models of chromium(VI) removal using *Phragmites australis and Ziziphus spina-christi biomass*

A. E. D. Mahmoud[1,2,3] · **M. Fawzy**[1,2,3] · **G. Hosny**[4] · **A. Obaid**[1]

Received: 3 July 2020 / Revised: 28 September 2020 / Accepted: 30 September 2020 / Published online: 14 October 2020

Abstract

In this study, we investigated the modeling of chromium (Cr(VI)) removal using globally available plant biomass: *Phragmites australis* and *Ziziphus spina-christi*. Biosorption parameters were initial Cr(VI) concentration (50–800 mg L^{-1}), contact time (1–180 min), adsorbent dose (0.25–2.0 g L^{-1}), and pH (2–8) at agitation speed of 100 rpm. Based on the results of batch experiments and modeling, pseudo-second-order model was fitted to the experimental data where $R^2 = 0.99$; besides, diffusion model played a significant role in the rate-determining step. Isotherm models were fitted in the order of Langmuir > Freundlich > Temkin models. Maximum adsorption capacities were recorded 21.32 mg g^{-1} and 15.55 mg g^{-1} for *Phragmites australis* and *Ziziphus spina-christi*, respectively. Insights into biosorption behavior were determined using Fourier-transform infrared spectra (FT-IR), scanning electron microscopy (SEM), and energy-dispersive X-ray spectroscopy (EDX). SEM–EDX revealed the chromium presence and its accumulation on both biosorbents after the biosorption process. Cr(VI) biosorption mechanism is illustrated and can be related to electrostatic interactions, reduction and chelation/complexation with the functional groups of both adsorbents.

Keywords Water treatment · Heavy metals · Leaf biomass · Adsorption · Isotherm · Removal mechanism

Introduction

Excessive use of heavy metals led their releasing into the environment through natural process and anthropogenic activities. Many industries in the worldwide such as leather, tanning, metallurgy, petrochemicals, battery, and paper manufacturing are mostly responsible of discharging various types of heavy metals into the environment.

Heavy metals pose a serious threat to human health because populations can be exposed to the heavy metals through water consumption. In addition, some heavy metals can bioaccumulate in the human bodies (e.g., in lipids and the gastrointestinal system) and provoke cancer and other health risks (Chowdhury et al. 2016).

Generally, wastewater effluents have different types of heavy metals. Removal of these heavy metals was successfully applied with adsorption technique as stated in the literature: cadmium (Mahmoud et al. 2016), copper (Barros et al. 2018), zinc, lead (Xu and McKay 2017), mercury (Wang et al. 2018), etc.

Herein, we focus on hexavalent chromium (Cr(VI)) whose concentration may vary from about ten to hundreds of ppm (mg L^{-1}) in the effluents of wastewater despite its

Editorial responsibility: Jing Chen.

Electronic supplementary material The online version of this article (https://doi.org/10.1007/s13762-020-02968-7) contains supplementary material, which is available to authorized users.

✉ A. E. D. Mahmoud
alaa-mahmoud@alexu.edu.eg

[1] Environmental Sciences Department, Faculty of Science, Alexandria University, 21511 Alexandria, Egypt

[2] Green Technology Group, Faculty of Science, Alexandria University, 21511 Alexandria, Egypt

[3] National Biotechnology Network of Expertise (NBNE), Academy of Scientific Research and Technology (ASRT), 11334 Cairo, Egypt

[4] Division of Environmental Health, Department of Environmental Studies, Institute of Graduate Studies and Research, Alexandria University, 21526 Alexandria, Egypt

maximum permissible limit of 0.05 mg L^{-1} in drinking water and 0.005 mg L^{-1} in irrigated water according to the World Health Organization. It is highly toxic because they are nonbiodegradable in nature and induce the toxic effects to living beings.

The variation of chromium concentration counts on the industrial sector (Kurniawan et al. 2011). In the leather and tanning industries, it is found that only 20% of the used chemicals are consumed and 80% of them are discharged in wastewater to reach aquatic environment (Laxmi and Kaushik 2020). The high concentrated chromium is due to the application of basic chromium sulfate ($Cr_2(SO_4)_3$) as a tanning agent.

The major issue with chromium is that it exists in a series of oxidation states ranged from − 2 to + 6. The most main states are trivalent Cr(III) species which are low soluble and low mobile and hexavalent Cr(VI) species which are highly soluble and mobile in our water bodies (Fawzy et al. 2016; Hlihor et al. 2017). Cr(III) is an essential trace element for the metabolism in mammals, whereas Cr(VI) is a toxic pollutant, teratogenic and carcinogenic (Mahmoud and Fawzy 2016; Pholosi et al. 2020a, b). Furthermore, Cr(III) can be easily oxidized to Cr(VI) which is more toxic to aquatic organisms (Mella et al. 2015; Yang et al. 2016).

In Egypt, Alexandria is one of the most important industrial cities, hosting about 60% of the national industries (Nasr et al. 2017). The suburban of Alexandria hosts approximately 40 tanneries. Unfortunately, these tanneries have no treatment plants and discharge their untreated or semi-treated effluents into the nearest sewerage system or directly into El-Max Bay west of Alexandria.

Consequently, the chromium removal from wastewaters is obligatory to mitigate and avoid water bodies pollution. From the literature survey, adsorption is a promising technique for heavy metals removal. Therefore, various biosorbents as pistachio hull (Moussavi and Barikbin 2010), broad bean shoots (Fawzy et al. 2016), *Magnolia* leaf (Mondal et al. 2019), and *Acacia auriculiformis* (Shahnaz et al. 2020) have been investigated for the removal of Cr(VI). All these reports indicated that the optimum Cr(VI) removal occurs in very acidic aqueous solutions (pH = 1–2), so the application of biosorption may not apply for the removal of other heavy metals or multi-metal solutions in the industrial sectors.

The objective of the proposed study is to investigate the biosorption performance of Cr(VI) from aqueous solutions using globally available and low-cost plant biomasses without modifications as *Phragmites australis* (Common reed) and *Ziziphus spina-christi* (Christ's thorn jujube) at higher pH values (4–6) than stated in the literature. *Phragmites australis* is chosen because it is distributed worldwide in general and specially in Alexandria City. It is the dominant species in the Lake Mariut representing 60% of the lake surface area. The mismanagement of *Phragmites australis* biomass would have negative impact on the lake ecosystem such as reducing the dissolved oxygen concentrations. *Ziziphus spina-christi* is selected because it is found in Africa and Asia and easily cultivated in dry and hot climates.

We focused on optimization of the experimental variables such as pH, contact time, biosorbent dosage, and Cr(VI) concentration on the biosorption process and validate various isotherm (highlight the sorption mechanism and the sorbent affinities) and kinetic models (prediction of the biosorption rate) including the intra-particle diffusion models that can be applicable for large-scale applications.

Materials and methods

Preparation of biosorbents

Phragmites australis (***Ph***) and *Ziziphus spina-christi* (***Zi***) were collected, during Autumn 2019, from the Botanical Garden of Faculty of Science, Alexandria University, Egypt. Plant specimens were dissected, cleaned, and rinsed with tap and double distilled water, followed by oven-drying at 60 °C for 72 h. After that, plant samples were crushed and ground by a stainless-steel grinder to a size of ≤ 250 µm. The resultant powder was stored in plastic bottles for further use.

Characterization of biosorbents

Fourier-transform infrared spectroscopy (FT-IR) of the investigated biomass after and before biosorption was carried out. The spectra were collected using PerkinElmer spectrum BX FT-IR system equipped with diffuse reflectance accessory within the range of 400–4000 cm^{-1}. A definite weight of each biomass was mixed with pure KBr and then compressed to form thin pellets (Mahmoud 2020a, b). Furthermore, the surface of the studied biosorbents before and after biosorption process was analyzed and photographed using a scanning electron microscope (SEM; JEOL—JSM-5300) equipped with energy-dispersive X-ray spectroscopy (EDX). Dried biomass of the studied biosorbents was mounted on copper stubs with double-sided adhesive tape and then analyzed for their relative metal contents by the EDX. Samples were then coated with 30 nm layer of gold using Polaron E5000 Sputter Coater, examined and photographed at 5000 magnifications by the SEM.

Experimental setup

A stock solution (2000 mg L^{-1}) of Cr(VI) ions was prepared by dissolving the required mass $K_2Cr_2O_7$ (analytical reagent grade) in double distilled water. Experimental Cr(VI) solutions of different concentrations were prepared by diluting the stock solution with suitable volumes of double distilled

water. The Cr(VI) concentrations were determined using a visible spectrophotometer (Pharmacia LKB-Novaspec) at $\lambda_{max} = 540$ nm using double distilled water as a blank. Its concept is based on reacting Cr(VI) with 1,5-diphenylcarbazide, which forms a red-violet-colored complex to be measured. The calibration curve is shown in Figure S1.

100 mL of a known Cr(VI) concentration solution was added into each flask, with a definite biosorbent mass. The suspension was stirred at 100 rpm using incubator shaker, HAF.Teck, Egypt. Different variables of biosorption process were investigated. The effects of biosorbents' doses (0.25–2 g L^{-1}), initial Cr(VI) concentrations (50–800 mg L^{-1}), and contact time (1–180 min) on Cr(VI) biosorption were studied. For pH adjustments, HCl (1 N)/NaOH (1 N) were used to study pH variable in the range of 2–8. All experiments were conducted in triplicate ± SD. Upon completion of the experimental trials, samples of the suspensions were withdrawn from the flasks and filtered through a fiberglass filter Whatman GF/A 47 mm (0.2 µm pore size) and the filtrate was analyzed for the residual Cr(VI).

Experimental calculations

Biosorption uptake capacities of Cr(VI) (q_e) onto the studied biosorbents were calculated according to Eq. 1 and the Cr(VI) removal efficiency (%R) was determined using Eq. 2 (Mahmoud et al. 2018a, b):

$$q_e = \left[\left(C_0 - C_e\right) \times V\right]/m, \tag{1}$$

$$\%R = \left[\left(C_0 - C_e\right)/C_0\right] \times 100, \tag{2}$$

where q_e is the quantity of solute adsorbed per unit weight of biosorbent (mg g^{-1}), C_0 is the initial Cr(VI) concentration (mg L^{-1}), C_e is the final equilibrium concentration of the Cr(VI) after biosorption (mg L^{-1}), m is the mass of biosorbent (g), and V is the volume of solution (L).

Pseudo-first-order (Eq. 3), pseudo-second-order (Eq. 4), and intra-particle diffusion (Eq. 5) models have been used to examine the mechanism and rate of the sorption process (Mahmoud and Fawzy 2016):

$$\mathrm{Log}\left(q_e - q_t\right) = \log q_e - \left[\left(k_1/2.303\right) \times t\right], \tag{3}$$

$$t/q_t = 1/k_2 q_e^2 + \left[\left(1/q_e\right) \times t\right], \tag{4}$$

$$q_t = \left(K_{id} \times t^{1/2}\right) + C_i \tag{5}$$

where q_t is the biosorption capacity at contact time (t), k_1 is the pseudo-first-order rate constant (min^{-1}), K_2 the pseudo-second-order rate constant (g mg^{-1} min^{-1}), K_{id} is the intra-particle diffusion rate constant (mg g^{-1} $min^{-1/2}$), and C_i is the intercept.

Additionally, isotherm models were taken into consideration. Langmuir sorption isotherm is often used to describe the maximum biosorption capacity. It can be represented by Eq. 6, whereas other isotherms as Freundlich and Temkin models are expressed by Eqs. 7 and 8, respectively:

$$C_e/q_e = 1/K_L q_{max} + C_e/q_{max} \tag{6}$$

$$\mathrm{Log}\left(q_e\right) = \log\left(K_f\right) + 1/n \times \log\left(C_e\right) \tag{7}$$

$$q_e = B\ \ln K_T + B\ \ln\ C_e, \tag{8}$$

where K_L is the Langmuir adsorption equilibrium constant related to the affinity between the Cr(VI) and biosorbents (L mg^{-1}), and $1/n$ is the heterogeneity factor of the adsorbent; it indicates the relative distribution of energy sites. Its value ranges between 0 and 1, indicating more heterogeneity as it gets closer to zero. K_f (mg g^{-1}) (L mg^{-1})$^{1/n}$ constant is concerned with the ability of biosorbent to adsorb. B is Temkin constant related to the heat of adsorption (J moL^{-1}); $B = RT/b$, K_T is the Temkin isotherm binding constant (L mg^{-1}), R is the ideal gas constant (8.314 J K^{-1} moL^{-1}), and T is the temperature in Kelvin.

Results and discussion

Characterization of biosorbents

Fourier-transform infrared spectra (FT-IR) of the raw plant biomasses (Fig. 1a, b) show predominant broad and strong peaks at 3428 and 3423 cm^{-1} in *Phragmites australis* ***(Ph)*** and *Ziziphus spina-christi* ***(Zi)*** biomass, respectively, representing O–H functional groups. There is also a band at 1512 in ***Ph*** biomass, and it is not detected in ***Zi*** biomass. It could be assigned to aromatic skeletal vibration of C=C representing the lignin presence. Moreover, bands displayed at 1642 cm^{-1} in ***Ph*** biomass and 1639 cm^{-1} in ***Zi*** biomass could be due to the presence of the carbonyl stretching bands (–C=O) (Nasr et al. 2017).

Subsequent to biosorption of Cr(VI), both biosorbents were dried and prepared again for FT-IR measurements in pellets forms. FT-IR spectra (Fig. 1a, b) demonstrated changes in the vibrational frequency of most functional groups. A pronounced shift was recorded for O–H stretching in alcohol/phenol group and primary and secondary amide bands. The O–H peaks shifted to 3454 cm^{-1} for ***Ph*** biosorbent and 3443 cm^{-1} for ***Zi*** biosorbent. Moreover, minor shift in the peaks was observed for –CH stretching, (–C=O) carbonyl stretching bands, (C–OH) carboxyl groups, and (C–N) primary amine stretching bands to 2921, 1642, 1319

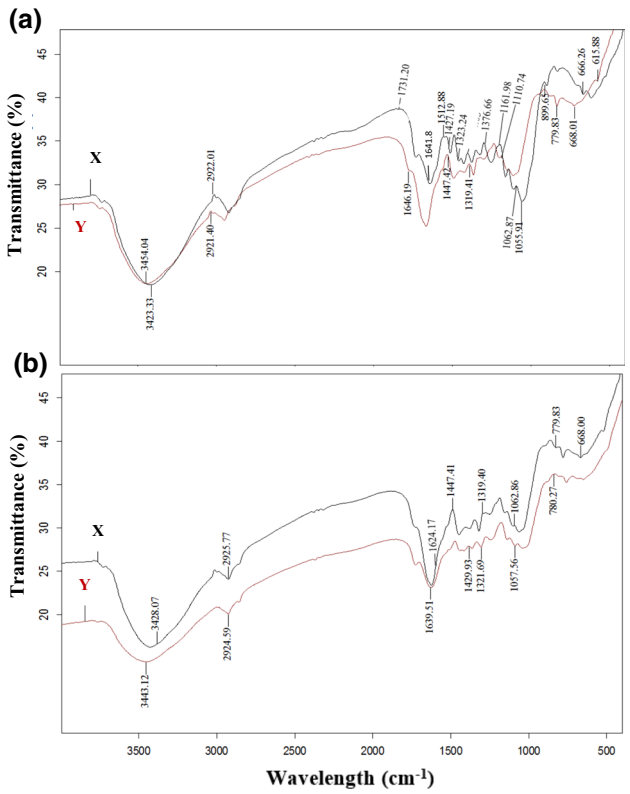

Fig. 1 FT-IR spectra of **a** *Phragmites australis* and **b** *Ziziphus spina-christi* before (*X*) and after (*Y*) Cr(IV) biosorption

and 1063 cm^{-1}, respectively, in ***Ph*** biosorbent, and 2924, 1639, 1322, and 1057 cm^{-1}, respectively, in ***Zi*** biosorbent. On the other hand, =CH binding band shifts to 805 cm^{-1} in ***Ph*** biosorbent, while to 780 cm^{-1} in ***Zi***, and the mono-substituted aromatic functional group was minor shifted in ***Ph*** to 669 cm^{-1}, whereas 680 cm^{-1} in ***Zi*** biosorbent due to the binding with Cr(VI).

The surface morphology of the studied biosorbents before and after Cr(VI) biosorption was obtained from scanning electron microscope (SEM). Figure 2a (left side) shows that the surface of ***Ph*** biomass has bigger pores than that of ***Zi*** biomass (Fig. 2c) and smooth, revealing substantial ability of adsorption due to high surface area. Hence, after the biosorption process (Fig. 2b; left side), its surface appears to be crammed with tiny granules in the cavities and on the surface, indicating the ability to sorb the Cr(VI) from the aqueous solution. Contrary to Fig. 2c, Fig. 2d (left side) shows that the surface of ***Zi*** biomass was filled with tiny granules after the biosorption process.

EDX proves our suggestion with the presence of Cr(VI) loaded on both biosorbents' surfaces. Figure 2a (right side) depicts the high peak of Cl ions followed by potassium (K) ions in the raw biomass of ***Ph***. On the other hand, the raw biomass of ***Zi*** possesses calcium (Ca) ions as the highest peak and medium peak of K ions (Fig. 2c; right side). Subsequent to the biosorption process, Fig. 2b, d (right side) indicates a substantial decrease in Ca, Cl, and K ions and appearance of dominating peak of Cr(VI) followed by another Cr(VI) peak at 5.5 keV. The same behavior was also reported by Duarte et al. (2012) and Kushwaha and Sudhakar (2013) with different biosorbents.

Optimization of experimental variables for Cr(VI) biosorption

All experiments were conducted at room temperature (25 ± 3 °C) for ease in the application at large scale and saving energy cost during the experimental work. Furthermore, equilibrium time of Cr(VI) biosorption was found independent on temperature as indicated in Mishra et al. (2015).

pH

Figure 3a, b shows the effect of pH on the uptake capacity (q_e) and removal percentage of 100 mg L^{-1} Cr(VI) in the range of pH 2–8. In the present study, it is proved that the amount and removal percentage of Cr(VI) decreased with the increase in solution pH. The optimum conditions of Cr(VI) uptake and removal were recorded at pH = 4 for *Ziziphus spina-christi* (***Zi***) and pH = 5 for *Phragmites australis* (***Ph***). This range of pH is in line with that reported by Chen et al. (2017) using different biosorbents for the Cr(VI) removal.

The low Cr(VI) biosorption at pH values higher than 6 is due to competition between OH^- and chromate ions; this leads to repulsion forces between chromium ions and biosorbents (Fawzy et al. 2016). The findings of Dawodu et al. (2020) showed that the amount and removal percentage of Cr(VI) sorbed on *Heinsia crinita* seed coat reduced with the rise in pH. Hence, the adequate pH for the further experiments with ***Ph*** and ***Zi*** biosorbents is 5 and 4, respectively.

Contact time

The determination of equilibrium time is vital for kinetic models. Therefore, the effect of contact time has been conducted for the investigated biosorbents. The removal percentage and q_e increased with increasing the contact time in the initial stage rapidly but became slow in the later stages till the attainment of equilibrium as illustrated in Fig. 4a, b. The equilibrium contact time between Cr(VI) and the studied biosorbents was 180 min. As time proceeds, the surface adsorption sites become exhausted leading to the

Fig. 2 SEM micrographs (left side) and EDX spectra (right side) of the investigated biosorbents: *Phragmites australis* biomass **a** before and **b** after Cr(VI) biosorption process and *Ziziphus spina-christi* biomass **c** before and **d** after Cr(VI) biosorption process

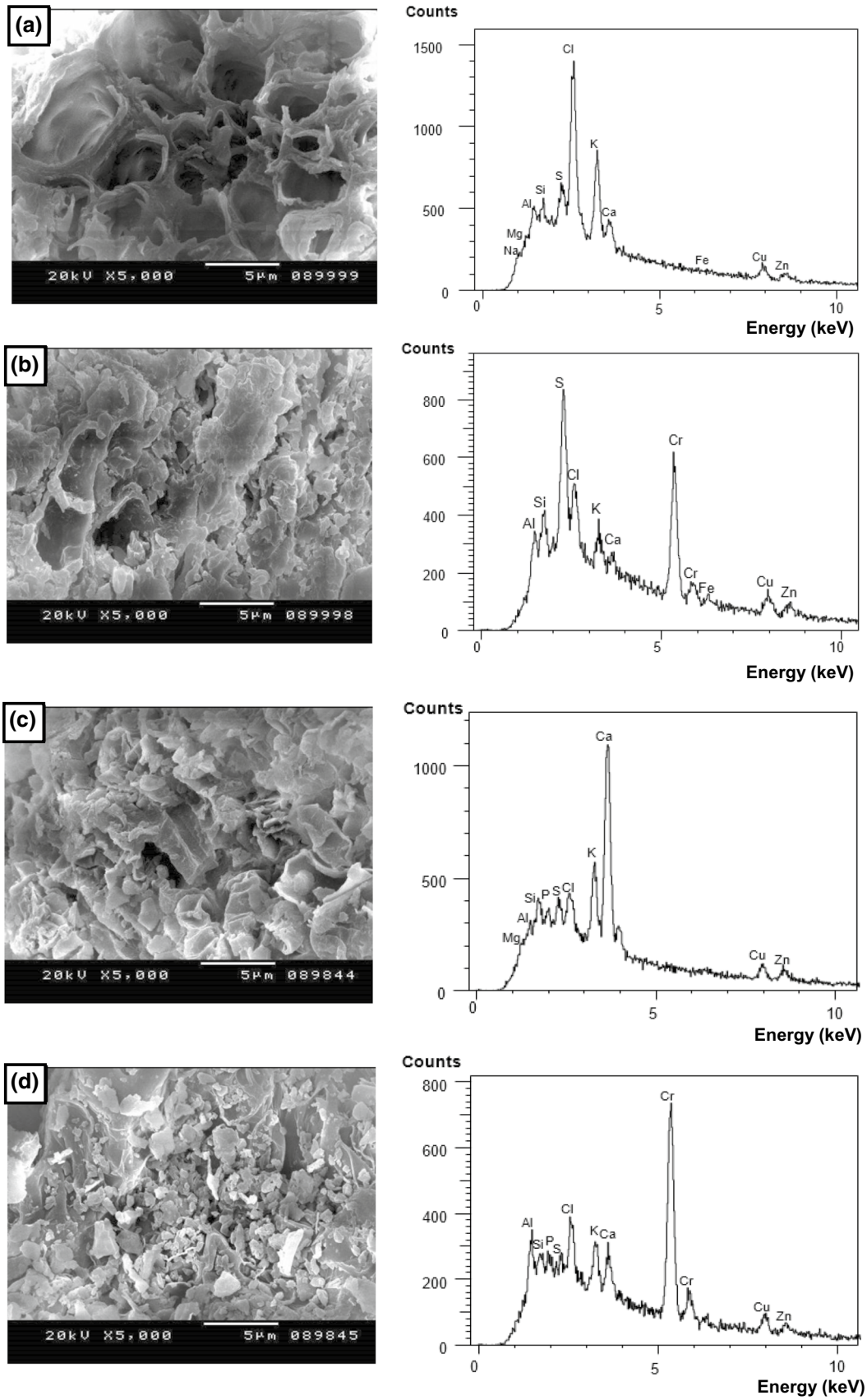
(a)
20kV X5,000 5µm 089999
Counts
Cl
K
S
Si
Al
Ca
Mg
Na
Fe
Cu
Zn
Energy (keV)
(b)
20kV X5,000 5µm 089998
Counts
S
Cr
Cl
Si
Al
K
Ca
Cr
Fe
Cu
Zn
Energy (keV)
(c)
20kV X5,000 5µm 089844
Counts
Ca
K
Si
P
S
Cl
Al
Mg
Cu
Zn
Energy (keV)
(d)
20kV X5,000 5µm 089845
Counts
Cr
Cl
Al
Si
P
S
K
Ca
Cr
Cu
Zn
Energy (keV)

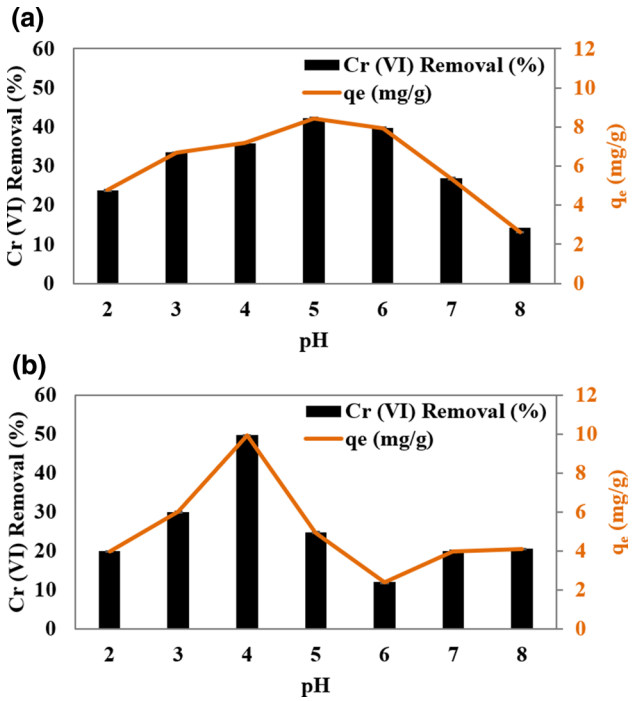

Fig. 3 Effect of pH on 100 mg L^{-1} of Cr(VI) removal with **a** *Phragmites australis* and **b** *Ziziphus spina-christi* at doses of 0.5 g L^{-1}; contact time = 180 min; temperature = 25 ± 3 °C

same sorption rate (Moussavi and Barikbin 2010; Ullah et al. 2013). It is relevant since the active sorption sites in the biosorbents have a fixed number and each active site can absorb only one ion in a monolayer sorption system. Subsequent to filling these active sites, their availabilities for the metal ions will be decreased and raising the competition in the aqueous solution for the metal ions removal (Ding et al. 2012).

Biosorbent dose

We investigated different biosorbent doses at the equilibrium time. Figure 5 illustrates the increment of Cr(VI) removal percentage from 41.4 to 84.3% with increasing the biosorbent dose of ***Ph*** from 0.25 to 2.0 g L^{-1}. On the other hand, the Cr(VI) removal percentage increased from 24.9 to 69.2% with ***Zi*** biosorbent.

The uptake sorption capacity of Cr(VI) ions showed the opposite behavior to the removal percentage as demonstrated in Fig. 5. The q_e value of ***Ph*** biosorbent decreased from 16.5 to 4.2 mg g^{-1} with increasing its dose gradually from 0.25 to 2.0 g L^{-1}. In the same contest, the q_e value of ***Zi*** biosorbent decreased from 9.9 to 3.45 mg g^{-1}. Such behavior is known in the biosorption process even with other biosorbents. Rathinam et al. (2010) demonstrated that an increase in the amount of seaweed *H. valentiae* from 4 to 8 g L^{-1} decreased the biosorption capacity of cadmium from 27.08 to 6.21 mg g^{-1}.

In the present account, the Cr(VI) removal using ***Ph*** and ***Zi*** biosorbents reached the maximum at 2.0 g L^{-1} = 84.30% and 69.2%, respectively. This can be because of increasing the biosorbent dose which provides more surface area and availability of more active sites, thus leading to the enhancement of metal ion removal (Mahmoud and Fawzy 2015; Mahmoud et al. 2016). However, above these doses, the percent removal tends to be constant or slightly decreased. This performance could be elucidated by the aggregates of the biosorbents at higher doses, which decreases the effective surface area for biosorption.

Initial Cr(VI) concentration

The initial sorbate concentration in the aqueous solution plays a key role as a driving force to overcome the mass

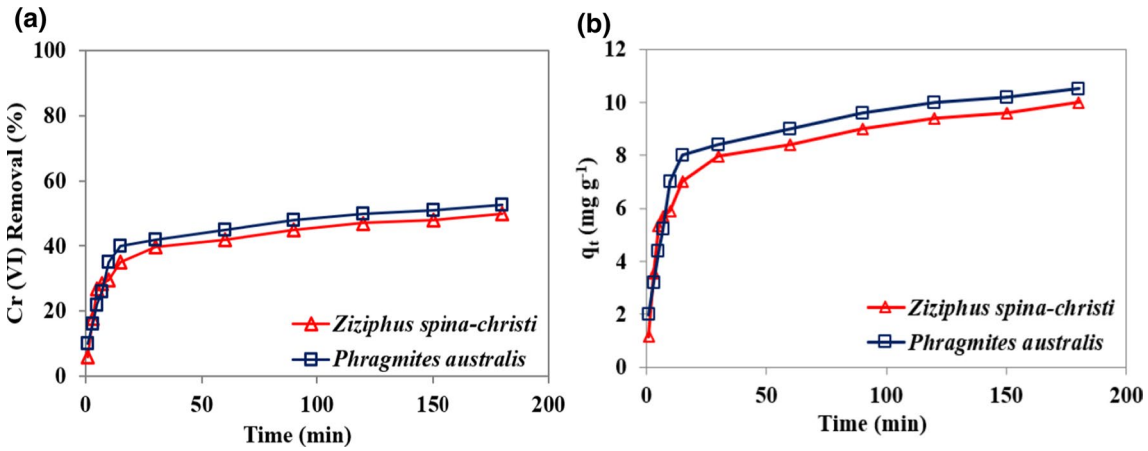

Fig. 4 Effect of contact time on **a** 100 mg L^{-1} Cr(VI) removal and **b** uptake capacity; q_t by the investigated biosorbents at doses of 0.5 g L^{-1}, pH = 5 for *Phragmites australis* and pH = 4 for *Ziziphus spina-christi*; temperature = 25 ± 3 °C

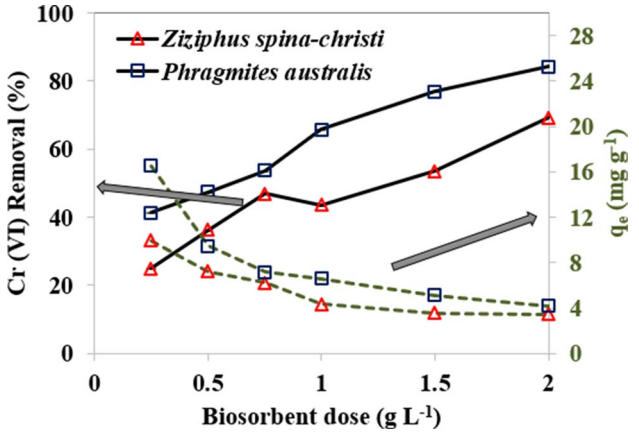

Fig. 5 Effect of biosorbent dose on 100 mg L^{-1} Cr(VI) removal and uptake capacity; q_e with pH = 5 for *Phragmites australis* and pH = 4 for *Ziziphus spina-christi* for 180 min; temperature = 25 ± 3 °C

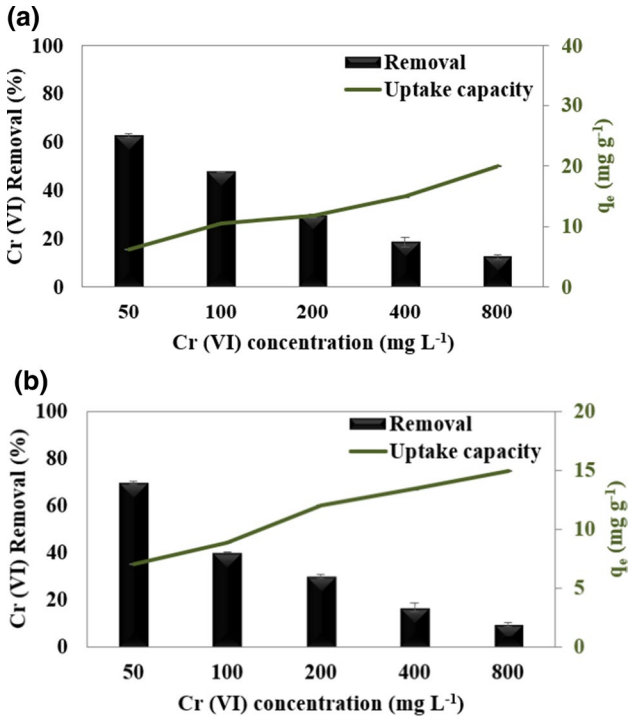

Fig. 6 Effect of Cr(VI) concentration on the performance of **a** *Phragmites australis* and **b** *Ziziphus spina-christi* with doses of 0.5 g L^{-1} at 180 min; pH = 5 for *Phragmites australis* and pH = 4 for *Ziziphus spina-christi*; temperature = 25 ± 3 °C

transfer resistance between the aqueous and solid phases (Mahmoud 2020a, b). Figure 6 shows the Cr(VI) uptake capacity (q_e) and its removal percentage at different initial Cr(VI) concentrations. ***Ph*** biosorbent recorded a decrement in the removal of Cr(VI) from 62.4% (6.2 mg g^{-1}) to 52.7% (10.5 mg g^{-1}) with the rise of its concentration from 50 to 100 mg L^{-1}. On the other hand, ***Zi*** biosorbent was able to remove 69.6% (6.9 mg g^{-1}) of 50 mg L^{-1} Cr(VI) and decreased to 50.0% (8.8 mg g^{-1}) with doubling the Cr(VI) concentration to be 100 mg L^{-1}.

It is also noted that the Cr(VI) removal steeply decreased from 29.4% (11.7 mg g^{-1}) to 12.5% (20.0 mg g^{-1}) using ***Ph*** biosorbent and 30.0% (12.0 mg g^{-1}) to 9.4% (14.9 mg g^{-1}) using ***Zi*** biosorbent when Cr(VI) concentration increased from 200 to 800 mg L^{-1}. Oves et al. (2013) and Pillai et al. (2013) reported that metal biosorption mechanism is practically dependent on the initial metal ions concentration. Generally, the increase in initial concentration of metal ions results in an increase in q_e and decreases in removal efficiency. This is a common phenomenon recorded for many biosorbents, e.g., *Pistachio* hull waste biomass (Moussavi and Barikbin 2010) and *Araucaria* leaves (Shukla and Vankar 2012). This is mainly because the transfer of metal ions from bulk solution to the surface of the sorbent increases with the increase in concentration of metal ions. It may be also due to improved collisions between Cr(VI) molecules as well as competition between the biosorbate ions for limited biosorbents surface. These forces lead to the enhancement of Cr(VI) sorption by both biosorbents. Therefore, the real industrial effluents should be diluted before being subjected to biosorption process in large-scale applications to obtain satisfied biosorption results with multi-metals in the effluents.

Kinetic models

Kinetic experiments were analyzed for their fitness with either pseudo-first-order or pseudo-second-order models to determine the kinetic order and rate constant of Cr(VI) biosorption onto the studied biosorbents.

Figure 7a reveals the variation of $\log(q_e - q_t)$ versus contact time. The linear fit gives a straight line with slope equal to the pseudo-first-order rate constant k_1 (min^{-1}) and intercept log q_e. Furthermore, Fig. 7b represents the linear plots of (t/q_t) versus time. The linear fit gives a straight line with slope of the rate constant ($1/q_e$) and intercept $1/k_2\ q_e^2$. The values of q_e, k_1, and k_2 including linear correlation coefficient R^2 are presented in Table 1.

In the present account, the fitness of the pseudo-second-order model has been confirmed with experimental results because it provides better correlation of the experimental data than the pseudo-first-order model. We found that the experimental and calculated q_e values from the pseudo-second-order kinetic model are very close to each other. Furthermore, the calculated correlation coefficients (R^2) are a closer to unity. The same findings were published by numerous researchers when using natural biosorbents for Cr(VI) removal (Pillai et al. 2013; Pholosi et al. 2020a, b; Prabhu et al. 2020).

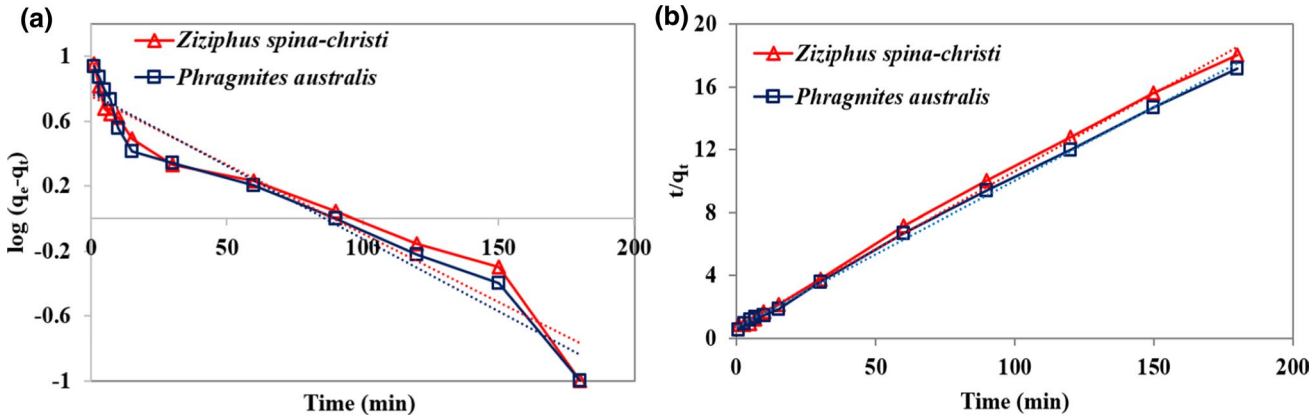

Fig. 7 **a** Pseudo-first-order and **b** Pseudo-second-order kinetic plots for biosorption of Cr(VI) onto the investigated biosorbents at doses of 0.5 g L^{-1}; pH = 5 for *Phragmites australis* and pH = 4 for *Ziziphus spina-christi*; temperature = 25 ± 3 °C

Table 1 Comparison between calculated and experimental uptake capacity (q_e) values of the investigated biosorbents for the kinetic models

Biosorbents	q_e (exp) mg g^{-1}	Pseudo-first-order model			Pseudo-second-order model		
		k_1 min^{-1}	q_e (calc) mg g^{-1}	R^2	k_2 g $mg^{-1}min^{-1}$	q_e (calc) mg g^{-1}	R^2
Phragmites australis (***Ph***)	10.5	0.020	5.86	0.94	0.24	10.60	0.99
Ziziphus spina-christi (***Zi***)	10.0	0.019	5.65	0.93	0.01	10.10	0.99

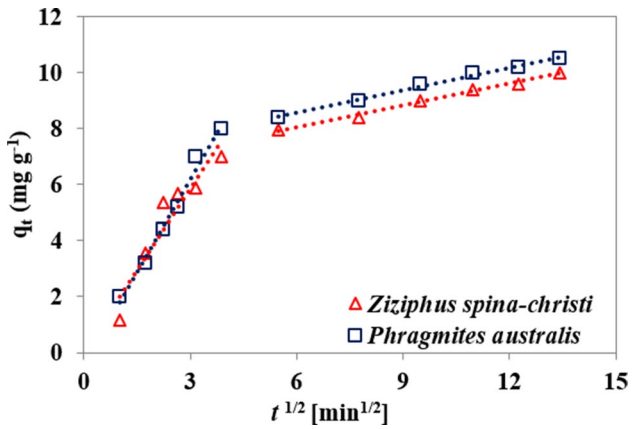

Fig. 8 Intra-particle diffusion models for the Cr(VI) biosorption using *Phragmites australis* and *Ziziphus spina-christi*

The aforementioned kinetic models cannot determine the rate and diffusion mechanisms. Hence, the model of intra-particle diffusion was investigated to check the metal uptake capacity versus the square root of time. As illustrated in Fig. 8, its plot did not pass through the origin (zero), indicating that this model was involved in the Cr(VI) biosorption but was not the only rate-limiting step (Pholosi et al. 2020a, b). The biosorption process has occurred in two stages (Fig. 8): (1) the initial stage is the film diffusion; transport of Cr(VI) from the aqueous solution to the external surface of the biosorbents, and (2) the second one is intra-particle diffusion where the diffusion of Cr(VI) takes place from the surface into the pores of the biosorbents.

The slopes (K_{1d} and K_{2d}) which point to the adsorption rate orders and the intercepts (C_1 and C_2) which highlight the surface biosorption of the intra-particle diffusion models are calculated in Table 2. The values of the adsorption rate order in the second phase (K_{2d}) are much smaller than K_{1d} because the resistance to mass transfer occurred in the second phase during the Cr(VI) diffusion into the investigated biosorbents. The intercepts (C_1 and C_2) of ***Ph*** biosorbent were higher than ***Zi*** biosorbent. Consequently, ***Ph*** biosorbent had more effect on the boundary layer.

Table 2 Intra-particle diffusion parameters for the Cr(VI) biosorption

Biosorbents	K_{1d} mg g^{-1} $min^{-1/2}$	K_{2d} mg g^{-1} $min^{-1/2}$	C_1	C_2	R_1^2	R_2^2
Phragmites australis (***Ph***)	2.208	0.267	0.38	6.97	0.986	0.991
Ziziphus spina-christi (**Zi**)	1.933	0.259	0.06	6.49	0.896	0.992

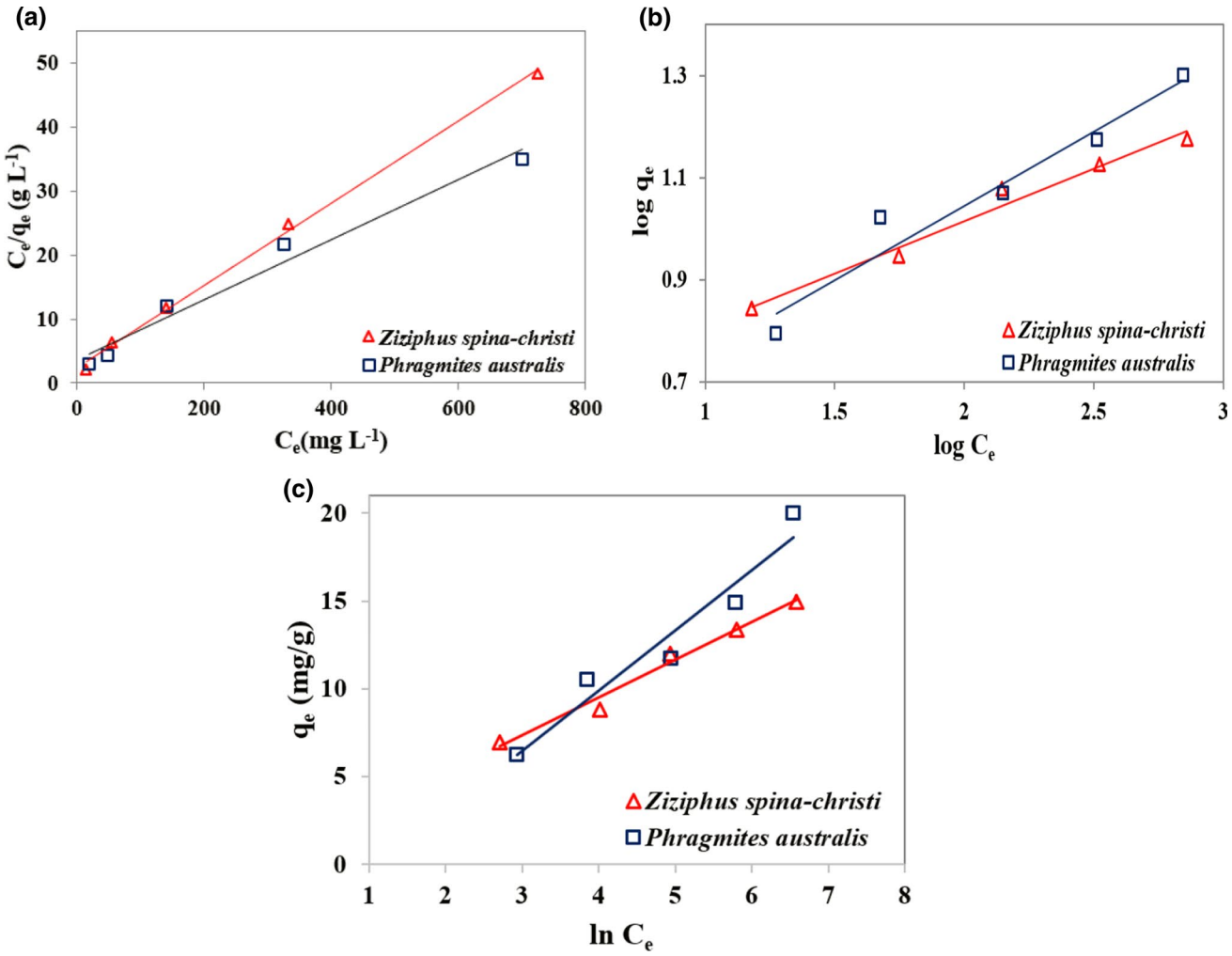

Fig. 9 Linear fit of **a** Langmuir, **b** Freundlich, and **c** Temkin isotherms at biosorbent dose = 0.5 g L^{-1}; pH = 5 for *Phragmites australis* and pH = 4 for *Ziziphus spina-christi* for 180 min; temperature = 25 ± 3 °C

Table 3 Langmuir, Freundlich, and Temkin biosorption isotherms of the investigated biosorbents for Cr(VI) biosorption

Biosorbents	Langmuir			Freundlich			Temkin		
	q_{max} (mg g^{-1})	K_L (L mg^{-1})	R^2	K_f	n	R^2	B	K_T (L mg^{-1})	R^2
Phragmites australis (***Ph***)	21.32	0.013	0.97	2.91	3.44	0.94	3.43	2.45	0.94
Ziziphus spina-christi (***Zi***)	15.55	0.027	0.99	4.04	4.88	0.97	2.15	10.63	0.98

Isotherm models

According to Fig. 9a–c, it can be pointed out that the biosorption isotherm can be fairly described by Langmuir rather than Freundlich and Temkin models. However, Langmuir and Freundlich isotherms can be applicable to the sorbent system denotes that both monolayer and heterogeneous surface conditions exist under the experimental conditions (Miretzky and Cirelli 2010; Moussavi and Barikbin 2010).

The affinity of the sorbed species is indicated by the coefficient K_L in the Langmuir model (Eq. 6). The lower value of K_L means the higher biosorption affinity of ***Ph*** biosorbent to Cr(VI) removal than ***Zi*** biosorbent as indicated in Table 2.

The constants of the isotherm models along with correlation coefficients for biosorption of Cr(VI) onto the investigated biosorbents are given in Table 3. q_m for ***Ph*** biosorbent was slightly superior to ***Zi*** biosorbent due to the shift amount in the carboxyl and carbonyl groups on the surface of each

Table 4 Review of Cr(VI) sorption using various biosorbents

Biosorbents	Conc. Cr(VI) (mg L^{-1})	Biosorbent dose (g L^{-1})	Contact time (min)	pH	Fitting models	Uptake capacity (mg g^{-1})	References
Date palm leaves	100	5	180	2	Langmuir	19.50	Fawzy et al. (2016)
Broad bean shoots				1	Langmuir	18.00	
Rye husk	260	10	140	3	Langmuir and reversible first order	22.62	Altun et al. (2016)
Chestnut oak shells	100	7	120	2	–	4.44	Niazi et al. (2018)
HCl-treated *Acacia nilotica* sawdust	100	2.9	80	6	Langmuir and pseudo-second-order	6.34	Khalid et al. (2018)
Formaldehyde-treated *Acacia nilotica* sawdust						8.20	
Walnut shell-activated carbon-supported Fe catalysts	100	10	400	2	Langmuir and pseudo-first-order	29.67	Derdour et al. (2018)
Sugarcane bagasse—granular activated carbon	10	–	180	6.2	Langmuir, Freundlich, and pseudo-second-order	9.75	Karri et al. (2020)
Ziziphus spina-christi	100	0.5	180	4	Langmuir, Freundlich, and pseudo-second-order	15.55	This study
Phragmites australis				5		21.32	This study

biosorbent which enhances electrostatic interactions between ***Ph*** biomass and Cr(VI). Furthermore, the high value of B (Temkin isotherm) in the case of ***Ph*** biosorbent indicates lower heats of adsorption with a higher surface coverage which proved that it has higher surface coverage for Cr(VI) biosorption than ***Zi*** biosorbent. The evaluated isotherm models had $R^2 > 0.94$ which validates their application to describe the Cr(VI) biosorption onto ***Ph*** and ***Zi*** biosorbents (Table 3).

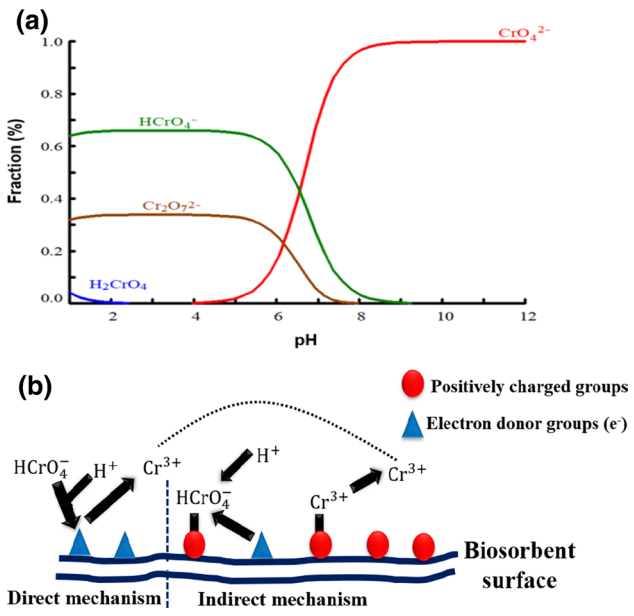

Fig. 10 **a** Speciation diagram of Cr(VI) species and **b** proposed adsorption-coupled reduction mechanisms of Cr(VI) by biosorbents

The difference in the performance of both plant biomasses in Cr(VI) removal is the higher lignin contents in ***Ph*** biomass than ***Zi*** biomass because of the high percentage of fibrous tissues. Despite the low biosorption capacity of ***Zi*** biomass, its antimicrobial potentials for water disinfection should be considered.

Compared to other biosorbents (Table 4), the uptake capacities of ***Ph*** and ***Zi*** biosorbents have similar or higher capacities than other biosorbents to remove Cr(VI) from aqueous solutions. Furthermore, the investigated biosorbents have the potential to be used without the need of carbonization step as compared in Table 4. This is an advantage to reduce the adsorption process cost and be an environmentally friendly technique.

Mechanism of Cr(VI) biosorption

The biosorption mechanism is reliant on the sorbate structure and the functional groups of the investigated biosorbents (Mahmoud et al. 2020). It is noted that speciation of Cr(VI) has a significant impact on its removal mechanism using biosorbents (Fig. 10a). In the range of pH = 1–6, $HCrO_4^-$ and dichromate ion ($Cr_2O_7^{2-}$) are the dominant species in equilibrium as also indicated in Jobby et al. (2018). Therefore, anionic adsorption mechanism was occurred where the negatively charged $HCrO_4^-$/$Cr_2O_7^{2-}$ are adsorbed to the positively charged functional groups of the studied biosorbents by electrostatic interactions. Based on Eqs. 9 and 10, $HCrO_4^-$ is reduced to Cr(III) at low pH. However, at pH higher than 6, $Cr(OH)_3$ is formed as an insoluble precipitate (Eq. 11):

$$Cr_2O_7^{2-} + 14H^+ + 6e^- \rightarrow Cr^{3+} + HCrO_4^- + 7H_2O \quad (9)$$

$$HCrO_4^- + 7H^+ + 3e^- \rightarrow Cr^{3+} + 4H_2O \quad (10)$$

$$CrO_4^{2-}/Cr_2O_7^{2-} + 4H_2O + 3e^- \rightarrow Cr(OH)_3 + 5OH^- \quad (11)$$

.

There are two mechanisms of "adsorption-coupled reduction" reactions as illustrated in Fig. 10b. Direct reduction mechanism occurs through the electron-donor groups of the studied biosorbents which possess less reduction potential values than that of Cr(VI) ions. Moreover, the reduced Cr(III) can either form complexes with the functional groups on the biosorbents or remain in the aqueous solution. Indirect reduction mechanism comprises three stages: (1) binding of anionic Cr(VI) to the positively charged functional groups of the biosorbents such as amino and carboxyl groups (Fig. 1), (2) reduction of Cr(VI) to Cr(III) by adjacent electron-donor groups, and (3) releasing Cr(III) into aqueous phase due to its repulsion with positively charged functional groups on the biosorbents or its complexation with adjacent groups.

Conclusion

Phragmites australis (***Ph***) and *Ziziphus spina-christi* (***Zi***) are efficient and cost-effective biosorbents for the removal of Cr(VI) from low- to medium-strength industrial wastewaters. EDX spectra of ***Ph*** and ***Zi*** biosorbents, after the biosorption process, confirm the presence of Cr(VI) loaded on biosorbents which is evidence that these biosorbents are effective in the removal of Cr(VI). The main functional groups that involved in the uptake of Cr(VI) are –OH, –CH, –C=O, C–OH, and C–N stretching bands.

The most important factor affecting the Cr(VI) biosorption is pH. The highest removal values of Cr(VI) were achieved at pH = 5 for ***Ph*** biosorbent, while pH = 4 for ***Zi*** biosorbent. We recorded the maximum sorption capacity (q_{max}) for ***Ph*** and ***Zi*** biosorbents at 21.32 and 15.55 mg g^{-1}, respectively. Such decrease in sorption capacity could be due to the unsaturated sorption sites during the sorption process.

The superior fitness of the pseudo-second-order model has been confirmed with experimental results because it provides better correlation of the experimental data than the pseudo-first-order model. ***Ph*** biosorbent had higher Cr(VI) surface coverage as proved by Temkin isotherm and SEM micrographs. Kinetic models illustrated that the adsorption process occurred in two phases: the film diffusion and intra-particle diffusion.

It is recommended that industrial effluents should be diluted before being subjected to biosorption process to obtain satisfied results. Further studies should be done to explore the performance of the investigated biosorbents with multi-metal solutions, and their regeneration for possible metals recovery should be investigated. Despite the low biosorption capacity of ***Zi*** biosorbent, its antimicrobial potentials for water disinfection should be considered.

Acknowledgements The first and second authors would like to thank the team of "Green Technology Group," Environmental Sciences Department and the research project entitled: Smart wireless sensor network to detect and purify water salinity and pollution for agriculture irrigation (SMARTWATIR), ERANETMED; Grant Number: 3.227. Furthermore, the support of Science, Technology, and Innovation Funding Authority (STDF-STIFA), Egypt, for the Project ID: 42961.

Compliance with ethical standards

Conflict of interest The authors declare no conflict of interest.

References

Altun T, Parlayıcı Ş, Pehlivan E (2016) Hexavalent chromium removal using agricultural waste "rye husk". Desalin Water Treat 57(38):17748–17756

Barros A, da Silva M, Kleinübing S (2018) Evaluation of copper and lead biosorption on modified azolla pinnata (r. Br.). Environ Eng Manag J (EEMJ) 17(1):83–94

Chen H, Dou J, Xu H (2017) Removal of Cr(VI) ions by sewage sludge compost biomass from aqueous solutions: reduction to Cr(III) and biosorption. Appl Surf Sci 425:728–735

Chowdhury S, Mazumder MJ, Al-Attas O, Husain T (2016) Heavy metals in drinking water: occurrences, implications, and future needs in developing countries. Sci Total Environ 569:476–488

Dawodu FA, Akpan BM, Akpomie KG (2020) Sequestered capture and desorption of hexavalent chromium from solution and textile wastewater onto low cost Heinsia crinita seed coat biomass. Appl Water Sci 10(1):1–15

Derdour K, Bouchelta C, Naser-Eddine AK, Medjram MS, Magri P (2018) Removal of Cr(VI) from aqueous solutions by using activated carbon supported iron catalysts as efficient adsorbents. World J Eng 15(1):3–13

Ding D-X, Liu X-T, Hu N, Li G-Y, Wang Y-D (2012) Removal and recovery of uranium from aqueous solution by tea waste. J Radioanal Nucl Chem 293(3):735–741

Duarte B, Silva V, Caçador I (2012) Hexavalent chromium reduction, uptake and oxidative biomarkers in halimione portulacoides. Ecotoxicol Environ Saf 83:1–7

Fawzy M, Nasr M, Abdel-Gaber A, Fadly S (2016) Biosorption of Cr(VI) from aqueous solution using agricultural wastes, with artificial intelligence approach. Sep Sci Technol 51(3):416–426

Hlihor RM, Figueiredo H, Tavares T, Gavrilescu M (2017) Biosorption potential of dead and living arthrobacter viscosus biomass in the removal of Cr(VI): batch and column studies. Process Saf Environ Prot 108:44–56

Jobby R, Jha P, Yadav AK, Desai N (2018) Biosorption and biotransformation of hexavalent chromium [cr (vi)]: a comprehensive review. Chemosphere 207:255–266

Karri RR, Sahu J, Meikap B (2020) Improving efficacy of Cr(VI) adsorption process on sustainable adsorbent derived from waste biomass (sugarcane bagasse) with help of ant colony optimization. Ind Crops Prod 143:111927

Khalid R, Aslam Z, Abbas A, Ahmad W, Ramzan N, Shawabkeh R (2018) Adsorptive potential of acacia nilotica based adsorbent for chromium(VI) from an aqueous phase. Chin J Chem Eng 26(3):614–622

Kurniawan A, Sisnandy VOA, Trilestari K, Sunarso J, Indraswati N, Ismadji S (2011) Performance of durian shell waste as high capacity biosorbent for Cr(VI) removal from synthetic wastewater. Ecol Eng 37(6):940–947

Kushwaha S, Sudhakar PP (2013) Sorption of uranium from aqueous solutions using palm-shell-based adsorbents: a kinetic and equilibrium study. J Environ Radioact 126:115–124

Laxmi V, Kaushik G (2020) Toxicity of hexavalent chromium in environment, health threats, and its bioremediation and detoxification from tannery wastewater for environmental safety. In: Saxena G, Bharagava RN (eds) Bioremediation of industrial waste for environmental safety: volume I: industrial waste and its management. Springer, Singapore, pp 223–243

Mahmoud AED (2020a) Eco-friendly reduction of graphene oxide via agricultural byproducts or aquatic macrophytes. Mater Chem Phys 253:123336. https://doi.org/10.1016/j.matchemphys.2020.123336

Mahmoud AED (2020b) Graphene-based nanomaterials for the removal of organic pollutants: insights into linear versus nonlinear mathematical models. J Environ Manag 270:110911

Mahmoud AED, Fawzy M (2015) Statistical methodology for cadmium (cd2+) removal from wastewater by different plant biomasses. J Bioremed Biodeg 6(304):2

Mahmoud AED, Fawzy M (2016) Bio-based methods for wastewater treatment: green sorbents. In: Ansari AA, Gill SS, GillG R, Lanza R, Newman L (eds) Phytoremediation: management of environmental contaminants, vol 3. Springer, Cham, pp 209–238

Mahmoud AED, Fawzy M, Radwan A (2016) Optimization of cadmium (cd^{2+}) removal from aqueous solutions by novel biosorbent. Int J Phytorem 18(6):619–625

Mahmoud AED, Stolle A, Stelter M (2018a) Sustainable synthesis of high-surface-area graphite oxide via dry ball milling. ACS Sustain Chem Eng 6(5):6358–6369. https://doi.org/10.1021/acssuschemeng.8b00147

Mahmoud AED, Stolle A, Stelter M, Braeutigam P (2018) Adsorption technique for organic pollutants using different carbon materials. In: Abstracts of papers of the American Chemical Society. Amer Chemical Soc 1155 16th st, NW, Washington, DC 20036 USA

Mahmoud AED, Franke M, Stelter M, Braeutigam P (2020) Mechanochemical versus chemical routes for graphitic precursors and their performance in micropollutants removal in water. Powder Technol 366:629–640. https://doi.org/10.1016/j.powtec.2020.02.073

Mella B, Glanert AC, Gutterres M (2015) Removal of chromium from tanning wastewater and its reuse. Process Saf Environ Prot 95:195–201

Miretzky P, Cirelli AF (2010) Cr(VI) and Cr(III) removal from aqueous solution by raw and modified lignocellulosic materials: a review. J Hazard Mater 180(1–3):1–19

Mishra A, Dubey A, Shinghal S (2015) Biosorption of chromium(VI) from aqueous solutions using waste plant biomass. Int J Environ Sci Technol 12(4):1415–1426. https://doi.org/10.1007/s13762-014-0516-0

Mondal NK, Samanta A, Roy P, Das B (2019) Optimization study of adsorption parameters for removal of Cr(VI) using magnolia leaf biomass by response surface methodology. Sustain Water Resour Manag 5(4):1627–1639

Moussavi G, Barikbin B (2010) Biosorption of chromium(VI) from industrial wastewater onto pistachio hull waste biomass. Chem Eng J 162(3):893–900

Nasr M, Mahmoud AED, Fawzy M, Radwan A (2017) Artificial intelligence modeling of cadmium(II) biosorption using rice straw. Appl Water Sci 7(2):823–831

Niazi L, Lashanizadegan A, Sharififard H (2018) Chestnut oak shells activated carbon: preparation, characterization and application for Cr(VI) removal from dilute aqueous solutions. J Clean Prod 185:554–561

Oves M, Khan MS, Zaidi A (2013) Biosorption of heavy metals by Bacillus thuringiensis strain OSM29 originating from industrial effluent contaminated north Indian soil. Saudi J Biol Sci 20(2):121–129

Pholosi A, Naidoo EB, Ofomaja AE (2020a) Batch and continuous flow studies of Cr(VI) adsorption from synthetic and real wastewater by magnetic pine cone composite. Chem Eng Res Des 153:806–818. https://doi.org/10.1016/j.cherd.2019.11.004

Pholosi A, Naidoo EB, Ofomaja AE (2020b) Intraparticle diffusion of Cr(VI) through biomass and magnetite coated biomass: a comparative kinetic and diffusion study. S Afr J Chem Eng 32:39–55. https://doi.org/10.1016/j.sajce.2020.01.005

Pillai SS, Mullassery MD, Fernandez NB, Girija N, Geetha P, Koshy M (2013) Biosorption of Cr(VI) from aqueous solution by chemically modified potato starch: equilibrium and kinetic studies. Ecotoxicol Environ Saf 92:199–205

Prabhu SG, Srinikethan V, Hegde S (2020) Pelletization of pristine pteris vittata l Pinnae powder and its application as a biosorbent of CD(II) and Cr(VI). SN Appl Sci 2(1):1–9

Rathinam A, Maharshi B, Janardhanan SK, Jonnalagadda RR, Nair BU (2010) Biosorption of cadmium metal ion from simulated wastewaters using hypnea valentiae biomass: a kinetic and thermodynamic study. Biores Technol 101(5):1466–1470

Shahnaz T, Patra C, Sharma V, Selvaraju N (2020) A comparative study of raw, acid-modified and EDTA-complexed acacia auriculiformis biomass for the removal of hexavalent chromium. Chem Ecol 36(4):1–22

Shukla D, Vankar PS (2012) Efficient biosorption of chromium(VI) ion by dry araucaria leaves. Environ Sci Pollut Res 19(6):2321–2328

Ullah I, Nadeem R, Iqbal M, Manzoor Q (2013) Biosorption of chromium onto native and immobilized sugarcane bagasse waste biomass. Ecol Eng 60:99–107

Wang T, Sun H, Ren X, Li B, Mao H (2018) Adsorption of heavy metals from aqueous solution by UV-mutant *Bacillus subtilis* loaded on biochars derived from different stock materials. Ecotoxicol Environ Saf 148:285–292

Xu M, McKay G (2017) Removal of heavy metals, lead, cadmium, and zinc, using adsorption processes by cost-effective adsorbents. In: Bonilla-Petriciolet A, Mendoza-Castillo DI, Reynel-Ávila HE (eds) Adsorption processes for water treatment and purification. Springer International Publishing, Cham, pp 109–138

Yang S, Jin P, Wang X, Zhang Q, Chen X (2016) Phosphate recovery through adsorption assisted precipitation using novel precipitation material developed from building waste: behavior and mechanism. Chem Eng J 292:246–254